Supplementary Materials for

Lignin: sustainable photothermal block for smart elastomers

Jinxing Li [a,#], Weifeng Liu [a,#,*], Xueqing Qiu [b], Xinpeng Zhao [c], Zhijun Chen [c,*], Mengzhen Yan [a], Zhiqiang Fang [d], Zhixian Li [a], Zhikai Tu [a], and Jinhao Huang [a]

[a] School of Chemistry and Chemical Engineering, Guangdong Engineering Research Center for Green Fine Chemicals, South China University of Technology, Wushan Road 381, Guangzhou, Guangdong, 510640, China.

[b] School of Chemical Engineering and Light Industry, Guangdong University of Technology, Guangzhou 510006, P. R. China.

[c] Engineering Research Center of Advanced Wooden Materials and Key Laboratory of Bio-based Material Science & Technology Ministry of Education, Northeast Forestry University, Harbin 150040, P. R. China.

[d] State Key Laboratory of Pulp and Paper Engineering and South China Institute of Collaborative Innovation, South China University of Technology, Wushan Road 381, Guangzhou, Guangdong, 510640, China.

[#] These authors contributed equally: Jinxing Li, Weifeng Liu.

*Corresponding authors E-mail: weifengliu@scut.edu.cn (W. Liu); chenzhijun@nefu.edu.cn (Z. Chen);

Materials and genernal methods

Materials. Alkali lignin (AL) (industrial grade) was provided by Shanghai Xufa new material Co., Ltd. (China) and was used directly without any purification or chemical modification. Enzymatic hydrolysis lignin (EL) was provided by Shandong Longli Co., Ltd. (China). Maleic anhydride grafted polyethylene elastomer (POE-MA GR209) was provided by Dow Chemical (USA). Stirling engine model, thermoelectric module, electric motor, water cooling plate and heat-sensitive metal sheet were purchased from Alibaba (Hangzhou, China). Escherichia coli and Staphylococcus aureus were provided by Guangdong Institute of Microbiology. The water used in the antibacterial experiments was deionized water.

Sample Preparation:

Low molecular weight alkaline lignin (AOH) was extracted from alcohol using AL as raw material. Firstly, the AL was dissolved in ethanol and filtered after mechanical stirring. The filtrate was concentrated to 300 ml after rotary evaporation. The concentrated solution was placed in a fume hood for 48 h and then transferred to a vacuum oven. The sample AOH was obtained by drying at 50 °C in vacuum.

AL and POE-MA were dried in vacuum oven at 50 °C for 24 h prior to use. POE-MA was first mixed in an internal mixer at 50 rpm and 100 °C for 15 min. Then preweighted AL was added and blended for another 15 min to prepare AL/POE composites. The samples were finally pressed into flat sheets with 1 mm thickness at 200 °C. The prepared samples were named as PxLy, with the numbers x, y representing the corresponding mass loadings of POE-MA, AL with the unit of g, respectively. P and L is an abbreviation of POE-MA and lignin, respectively.

Characterizations:

Ultraviolet-visible-near-infrared spectra (UV-Vis-NIR) were collected on a Lamdba 950 UV-Vis-NIR spectrometer (Platinum Elmer Instruments Co., Ltd., USA) in order to test the light absorption of lignin at 200-1250 nm.

To monitor the photothermal temperature changes of lignin and lignin/POE composite elastomers, a 808 nm semiconductor laser emitter (Lasever Inc., China) was used as the light source, and an infrared camera (FLIR Systems, Inc., USA) was used as temperature detection equipment to monitor the temperature change. A xenon lamp (Beijing Perfectlight Technology Co., Ltd) was also used to monitor the solar light. The power density ($W \cdot cm^{-2}$) refers to the light intensity irradiated on the sample per unit area (cm^{-2}), which was adjusted by the distance between light source and sample and was tested by optical power meter (PL-MW 2000, Beijing Perfectlight Technology Co., Ltd). The temperature data were collected every 10s, a temperature rise and fall cycle was set to 7 min (heating 4 min and cooling 3 min).

The fluorescence emission spectrum and phosphorescence emission spectrum of AL was determined on a U-3900 ultraviolet spectrophotometer to infer the main energy dissipation form after AL absorbs light. The excitation wavelength was selected as 808 nm, and the emission wavelength in the range of 830-900 nm was collected.

The specific heat capacity of AL, the melting point and specific heat capacity of AL/POE composites were determined on a DSC 2500 calorimeter (TA instrument, USA). The melting point was tested as follows: The temperature was first increased to 160 °C at a heating rate of 50 °C min^{-1}, and was kept constant for 3 min to eliminate the thermal history. Then the temperature was reduced to -85 °C at a rate of 10 °C min^{-1}, and was kept constant for 3 min. Finally the temperature was increased to 160 °C at a rate of 10 °C min^{-1}. The crystallization temperature (T_c) and melting temperature (T_m) were obtained from the second heating process.

The specific heat capacity test procedure was as follows: The temperature was first set to 20 °C,

kept constant for 5 min, then raised to 250 °C at 5 °C min^{-1}, and kept constant temperature for 5 min. The specific heat capacity was collected from the temperature range of 20~250 °C.

The quantitative shape memory effect of composite elastomer was tested on a dynamic mechanical analyzer (DMA 850, TA instrument, USA). The test procedure was as follows: (1) The prestress was set to 0.0001 N, and the temperature was raised to 90 °C at a rate of 10 °C·min^{-1}, and was kept constant for 4 min; (2) A stress of 0.35 MPa was applied for 3 min; (3) The stress was maintained at 0.35 MPa, and the temperature was reduced to 0 °C at a rate of 10 °C·min^{-1}, and was kept at 0 °C for 3 min; (4) The stress was removed and the temperature was kept at 0 °C for another 2 min; (5) The temperature was rose to 90 °C at a rate of 10 °C·min^{-1}, and was maintained at 90 °C for 20 min.

Dumbbell-shaped samples were cut into a length of 75 mm and a neck width of 4 mm for tensile tests. The engineering stress-strain curves were determined on CMT 4204 electronic universal testing machine (MTS Systems Co. Ltd, China) according to the standard GB/T 1040-2006 at a loading speed of 200 mm min^{-1} at 25 °C under a relative humidity of 40±5%. The mechanical properties before and after self-repairing were compared to evaluate the self-repairing efficiency of the material.

A wound of ~1 mm width × 1 mm depth was cut with a scalpel in the middle of the dumbbell-shaped sample to imitate the actual damage of the material. A 808 nm near-infrared laser with a power density of 1.61 W cm^{-2} was used to irradiate the damaged part. The tensile stress-strain curves of the repaired dumbbell-shaped sample were tested. The micro-morphology of the damaged area before and after self-repairing was observed by a polarizing microscope (BIMU Instrument Co., Ltd, China) and also by scanning electron microscope (FE-SEM, HITACHI SU-8220, Japan).

P32L8 composite film with size of 25 mm × 25 mm was put into the cylinder of the Stirling engine model to display the photo-thermal-mechanical conversion. The composite film was

irradiated with a xenon lamp or near-infrared laser. AL absorbed light energy and converted it into heat energy. The emitted heat caused the air in the cylinder to expand, which in turn pushed the piston to move. The rotation of the engine flywheel under different conditions was recorded. The control experiment was conducted with pure POE film without AL.

The P32L8 film, thermoelectric module, and water-cooled plate were connected together to form a thermoelectric generator (TEG) to test the photo-thermal-electric conversion. The xenon lamp irradiated the polymer film, which would cause a temperature difference between the two sides of the thermoelectric module. Based on the Seebeck effect, electrical energy was generated, and the power was supplied to an electric fan. The power density of the xenon lamp was adjusted, the voltage change could be expressed by the voltmeter and the fan speed. The control experiment was conducted with pure POE film for comparison.

The P32L8 film was placed tightly on the surface of the heat-sensitive metal sheet and a simple loop with the DC power supply was constructed to test the photothermal control switch. The P32L8 film was irradiated with a certain intensity of near-infrared light (0.83 W cm^{-2}), the AL in the composite material absorbed heat energy and converted it into heat energy, finally made the heat-sensitive metal sheet reaching the trigger temperature (30 °C) and realized the remote control on the switch on/off of the circuit.

The conventional antibacterial zone method was used to determine the photothermal antibacterial ability of the P32L8 composite film. 75% Ethanol solution and ultraviolet lamp were used to sterilize the polymer film with a diameter of about 6 mm and a thickness of about 1 mm before the tests. The initial bacterial solution was added to the Luria-Bertani (LB) liquid medium. Then it was placed in a 37 °C incubator for 6 hours to make the number of colonies meet the requirements for use (the required number of colonies was about $1*10^{8}$ mL^{-1}). The cultured bacterial species were centrifuged to remove the nutrient components of the medium, and then an equal amount of sterile water was added to prepare a bacterial solution for later use. The sterilized

polymer film (P32L8) was put into the well plate with 150 μL of bacterial solution. Near-infrared laser light (1.61 W cm^{-2}) was on for 5 minutes. The obtained bacterial suspension was diluted 10^5 times. Then we took 100 μL of the medium and placed it on the LB agar plate. Finally, the LB plate was placed in a 37 °C incubator for 20 hours, and the colony forming unit (CFU) was calculated to obtain the sterilization rate. The effective CFU results were between 30 and 300. A bacterial suspension with POE film was used as a control. The bactericidal ratio was calculated as (CFU of control-CFU of P32L8 film sample) / CFU of the control.

Simulation methods:

In this work, the density functional theory (DFT) calculation was performed using the Dmol[3] code.[1] The exchange-correlation interaction was treated by the generalized gradient approximation (GGA) with PBE functional.[2] A double numerical quality basis set with d-type polarization function (DNP)[3] was utilized for all the geometric optimizations, total energy calculations. The core electrons were modelled using effective core pseudopotentials (ECP) by Dolg[4] and Bergner.[5] Grimme's semi-empirical DFT-D[6] was introduced in the computations to guarantee a better description of the electron interaction in a long range. All calculations were performed spin unrestricted. The real space cutoff radius was 0.37 nm. The convergence tolerance for SCF was 1.0×10^{-6} Ha. Those of geometry optimization for energy and maximum force were 1.0×10^{-5} Ha and 0.002 Ha/Å, respectively. The binding energy (E_b) is defined as: $E_b = E_{A+A} - 2E_A$, where E_{A+A} is the total energy of combined two A, E_A is the total energy of a single A. A refer to AOH, AL and EL, respectively.

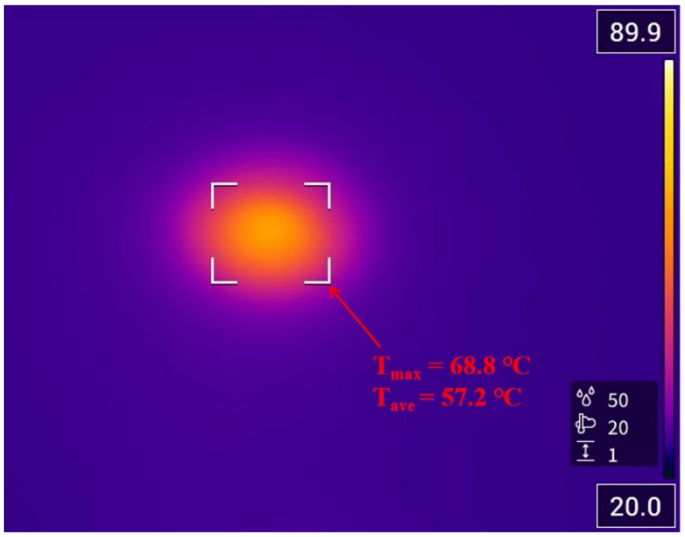

Fig. S1 IR images of AL irradiated under 0.1 W·cm^{-2} xenon lamp captured by IR camera.

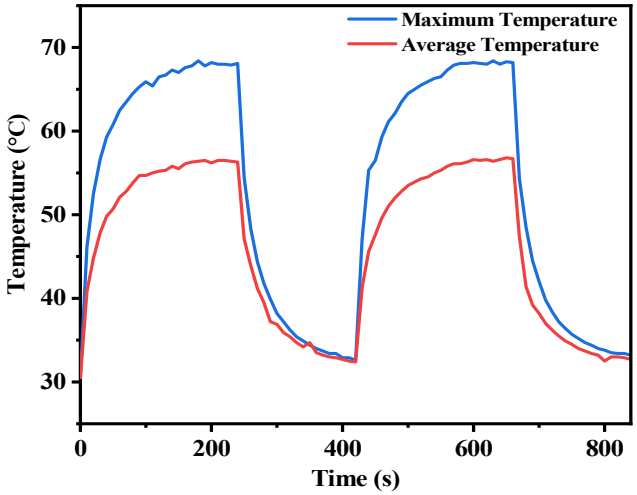

Fig. S2 The heating and cooling cycle of AL after irradiation with xenon lamp (0.1 W·cm^{-2}).

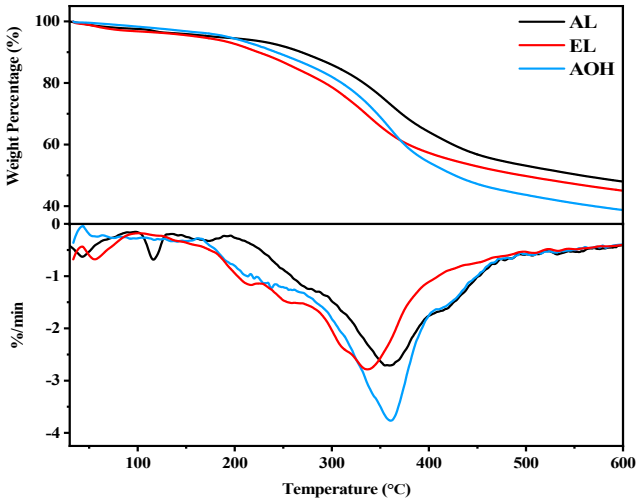

Fig. S3 TGA and DTG curves of AL, EL, AOH.

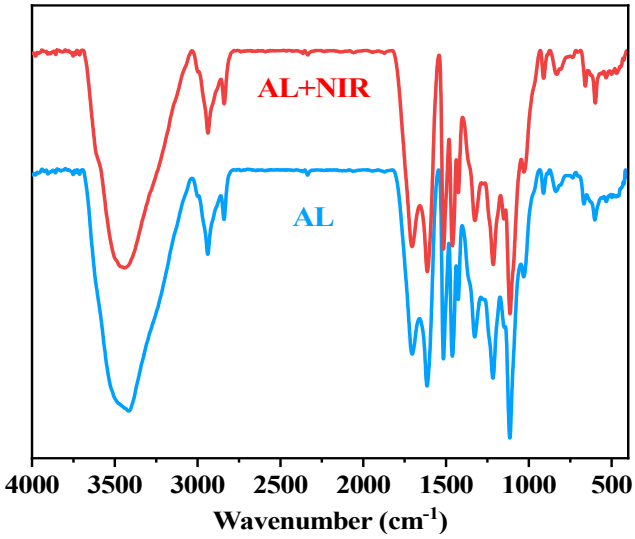

Fig. S4 FTIR spectra of different samples before and after 1.25W·cm^{-2} illumination: AL, AL+NIR.

The photothermal conversion efficiency was determined according to previous method[7-9]. Details are as follows:

Based on the total energy balance for this system:

$$\sum_i m_i C_{p,i} \frac{dT}{dt} = Q_s - Q_{loss} \quad \text{(S1)}$$

where m_i and $C_{p,i}$ are the mass and heat capacity of sample (AL or P32L8), respectively. Q_s is the photothermal heat energy input by irradiating NIR laser to samples, and Q_{loss} is thermal energy lost to the surroundings.

Thermal energy lost to the surroundings Q_{loss} is calculated according to the following formula:

$$Q_{loss} = hS(T - T_{surr}) = hS\Delta T \quad \text{(S2)}$$

Where h is the heat transfer coefficient, S is the surface area of the container.

When the temperature reaches the maximum value, the system is in balance.

$$Q_s = Q_{loss} = hS(T_{\max} - T_{surr}) = hS\Delta T_{\max} \quad \text{(S3)}$$

ΔT_{max} is the maximum steady-state temperature change. The light-to-heat conversion efficiency η is calculated according to the following formula:

$$\eta = \frac{hS\Delta T_{\max}}{I} \quad \text{(S4)}$$

where I is the laser power (0.344 W) .

In order to obtain the hS, a dimensionless driving force temperature, θ is introduced as follows:

$$\theta = \frac{T - T_{surr}}{T_{\max} - T_{surr}} \quad \text{(S5)}$$

$$d\theta = \frac{1}{T_{\max} - T_{surr}} dT = \frac{1}{\Delta T_{\max}} dT \tag{S6}$$

where T is the temperature of sample, T_{max} is the maximum steady-state system temperature, and T_{surr} is the initial temperature. Then substituting Eq. S6 into Eq. S1 and rearranging to get:

$$\frac{d\theta}{dt} = \frac{hS}{\sum_i m_i C_{p,i}} \left(\frac{Q_s}{hS\Delta T_{\max}} - \frac{\Delta T}{\Delta T_{\max}} \right) \tag{S7}$$

The sample system time constant τ_s:

$$\tau_s = \frac{\sum_i m_i C_{p,i}}{hS} \tag{S8}$$

So we can get:

$$\frac{d\theta}{dt} = \frac{1}{\tau_s} \frac{Q_s}{hS\Delta T_{\max}} - \frac{\theta}{\tau_s} \tag{S9}$$

when the laser is off, $Q_s = 0$, therefore

$$\frac{\mathrm{d}\theta}{\mathrm{d}t} = -\frac{\theta}{\tau_s} \tag{S10}$$

$$t = -\tau_s \ln \theta \tag{S11}$$

Take t as the y-axis and lnθ as the x-axis to plot, and the cooling time τ_s can be obtained from the slope. Finally get the photothermal conversion efficiency η of the sample.

Choose a normal heating and cooling cycle for the calculation of the photothermal conversion efficiency of AL, and select the data points in the cooling section of the average temperature recorded by the infrared camera for calculation. According to Fig. S5, the cooling time constant of AL was obtained τ_s = 22.57 s. Integral specific heat capacity C_p = 1.263 J $(g \cdot °C)^{-1}$. Other parameters of AL: m_i = 0.025 g. Finally, the photothermal conversion efficiency of AL is calculated to be 48.8%.

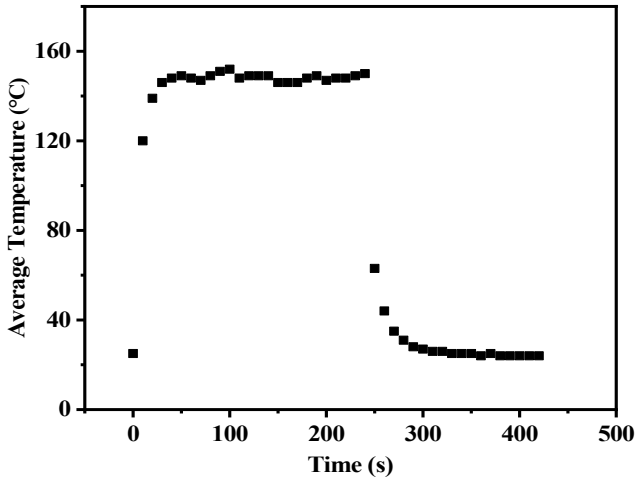

Fig. S5 The heating and cooling cycle of AL after irradiation with 808 nm laser (1.25 W cm^{-2}).

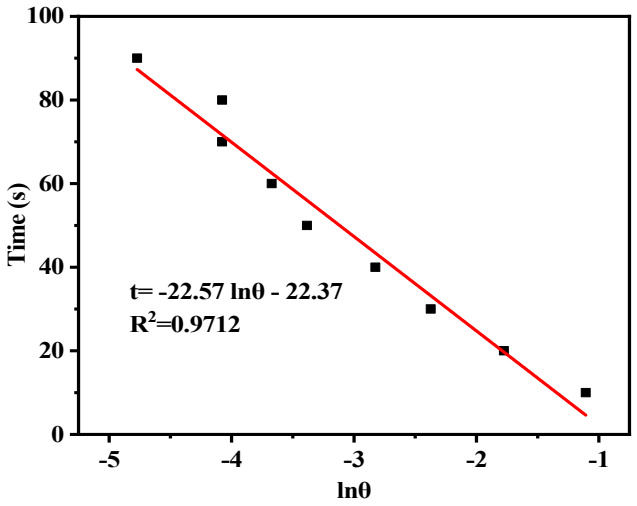

Fig. S6 The corresponding time-lnθ linear curve of the heating and cooling cycle of AL.

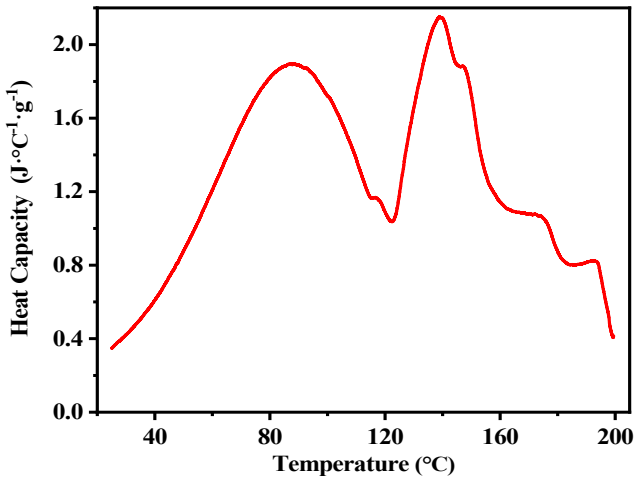

Fig. S7 The change of specific heat capacity of AL from 25 °C to 200 °C with DSC instrument.

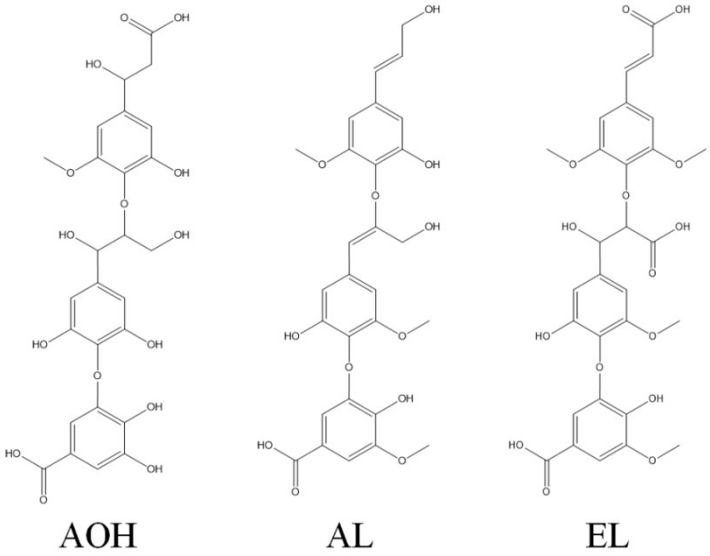

Fig. S8 The molecular structure of model AOH (left), AL (middle) and EL (right).

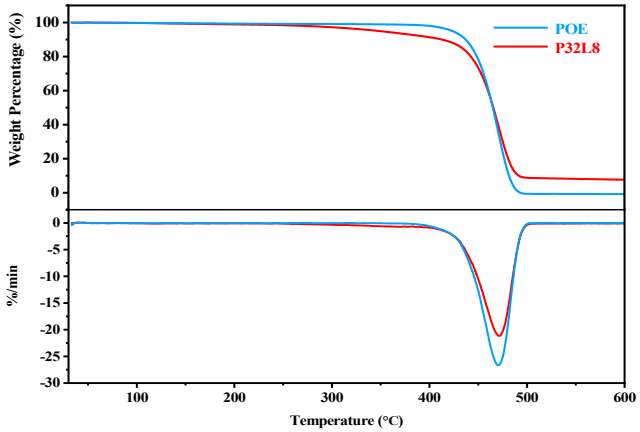

Fig. S9 TGA and DTG curves of pure POE and the composite elastomer P32L8.

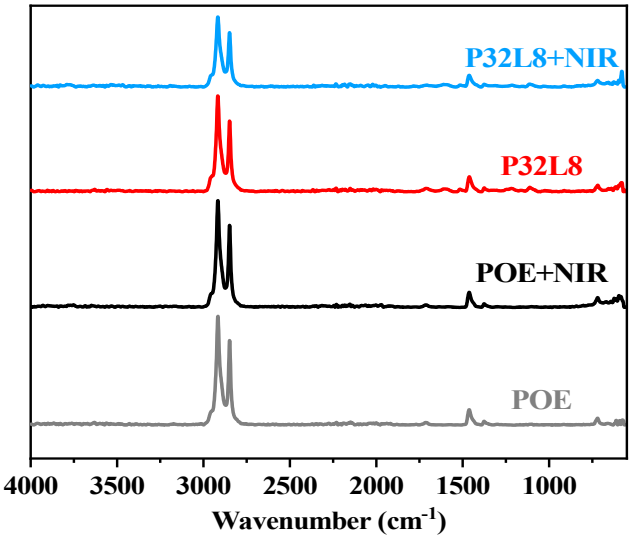

Fig. S10 Infrared spectra of different samples before and after 1.25W cm^{-2} illumination: POE, POE+NIR, P32L8, P32L8+NIR.

Calculation of photothermal efficiency of composite materials:

A normal light heating/cooling cycle was chose as the calculation of the P32L8 photothermal conversion efficiency, and the data points in the cooling section of the average temperature recorded by the infrared camera were selected for calculation. According to Fig. S8, the cooling time constant of P32L8 was obtained τ_s=25.5 s. Integral specific heat capacity C_p=1.912 J $(g\cdot°C)^{-1}$, Other parameters of P32L8: m_i = 0.0152 g, Finally, the photothermal conversion efficiency of P32L8 was calculated to be 40.2%.

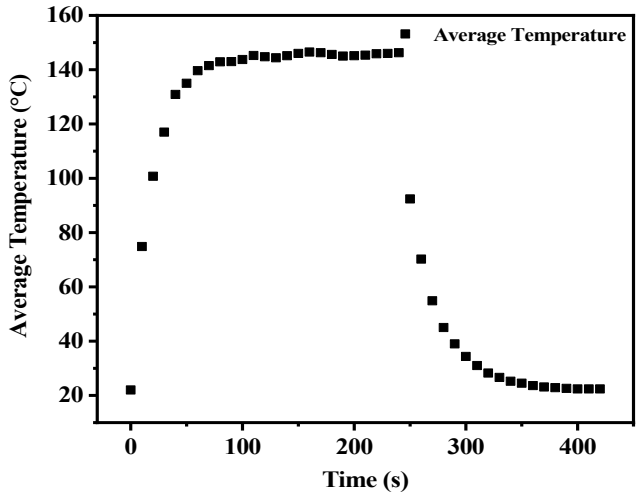

Fig. S11 The heating and cooling cycle of P32L8 after irradiation with 808 nm laser (1.25 W·cm^{-2}).

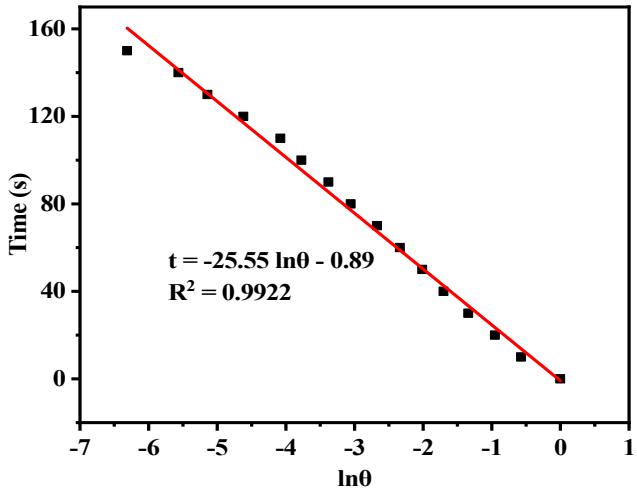

Fig. S12 The corresponding time - lnθ linear curve of the heating and cooling cycle of P32L8.

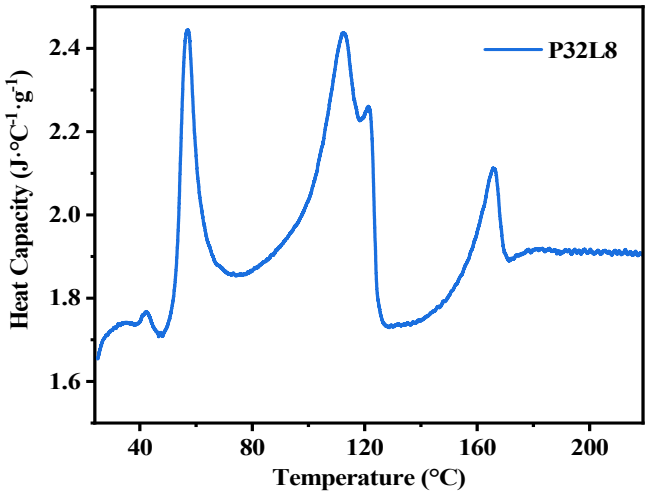

Fig. S13 The change of specific heat capacity of P32L8 at 25 °C-220 °C with DSC instrument.

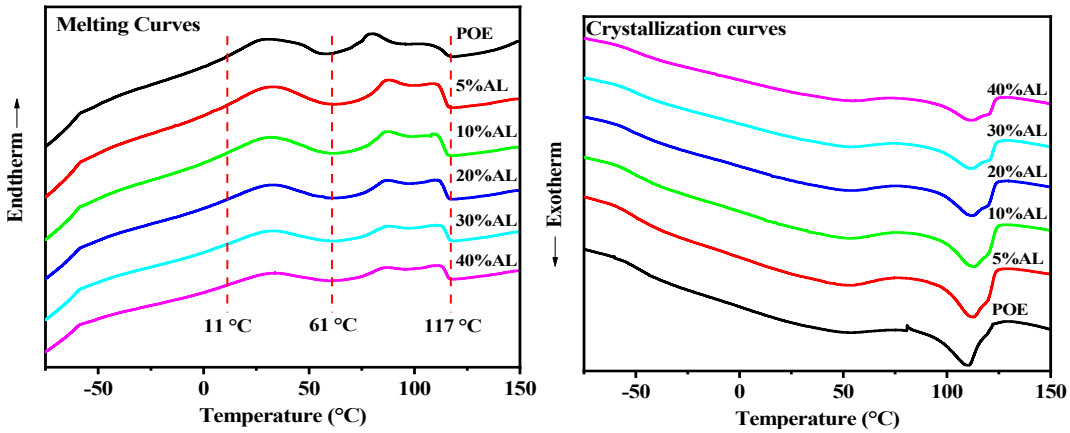

Fig. S14 (a) melting curves and (b) crystallization curves of AL/POE composite elastomers.

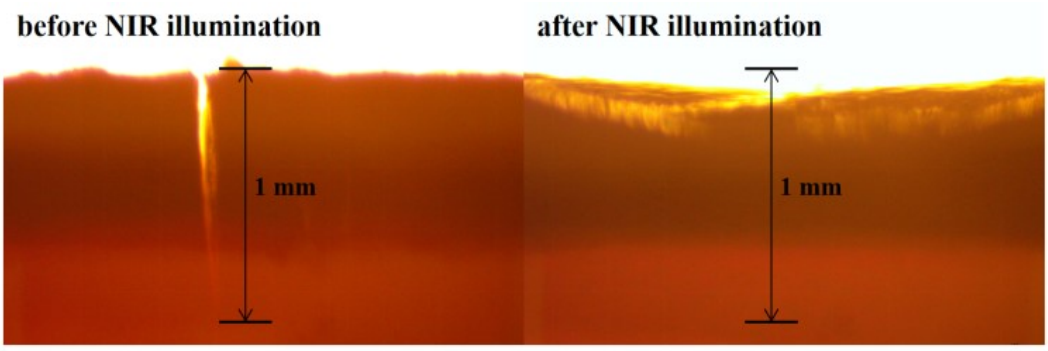

Fig. S15 A partial enlarged view on the wound before and after NIR illumination taken by an optical microscope.

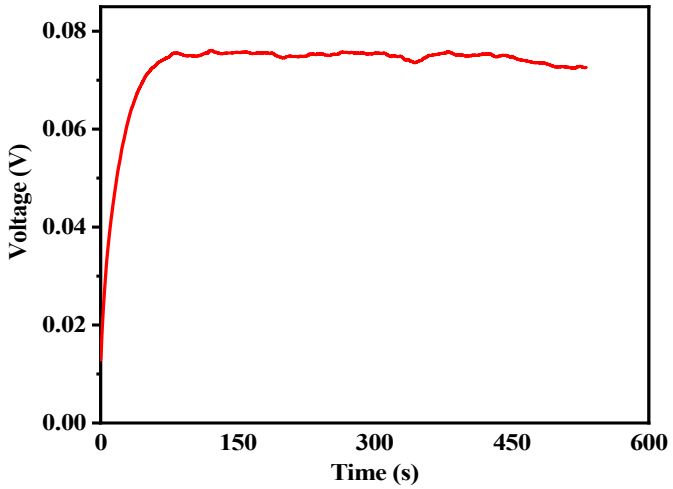

Fig. S16 The voltage of TEGS driven by solar energy generated by POE film under light irradiation (0.1 W cm^{-2}).

Benefiting from the good photothermal conversion effect of lignin, the composite elastomer P32L8 could also be used for photothermal control switch under the illumination of NIR light laser, as verified in Fig. S15. The photothermal control switch was designed in a circuit, as shown in Fig. 15a and b, where the P32L8 film was tightly attached on the surface of the heat-sensitive metal sheet. Under the illumination of the NIR laser, the lignin in the composite converted the light energy into heat, which made the heat-sensitive metal sheet responding to the trigger temperature (30 °C), so as to realize the switch on/off in the circuit by illumination (**Movie S11**). The remote control of the photothermal switch could be further applied to new uses such as smart alarm systems, etc.

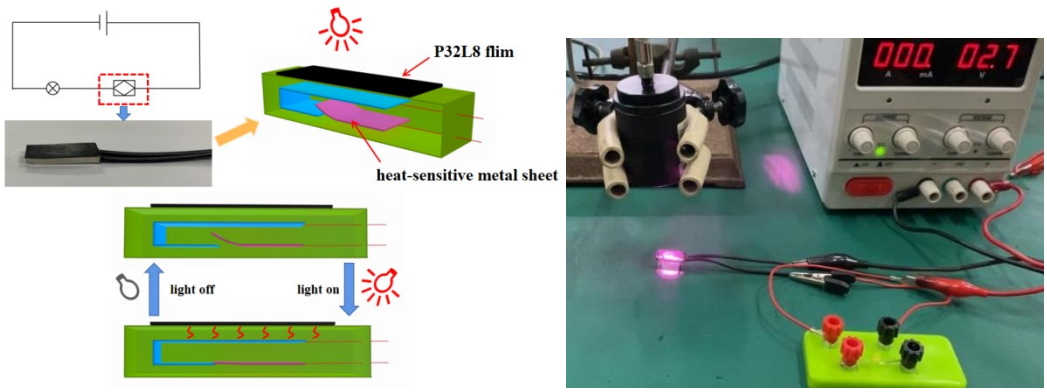

(a) **(b)**

Fig. S17 (a) The circuit diagram of the photothermal control switch. (b) The picture of the photothermal control switch, where the P32L8 film was tightly attached to the surface of the heat-sensitive metal. The heat-sensitive metal could respond to the trigger temperature of 30 °C.

Movie S1.
Infrared thermal imaging images of AL under NIR light irradiation (1.25W cm^{-2}, 808 nm）
Movie S2.
Infrared thermal imaging images of P32L8 under NIR light irradiation (1.25W cm^{-2}, 808 nm）
Movie S3.
Infrared thermal imaging images of POE under NIR light irradiation (1.25W cm^{-2}, 808 nm）
Movie S4.
Visual demonstration of the shape memory effect of P32L8 film under NIR light irradiation (0.47 W cm^{-2}, 808 nm)
Movie S5.
Infrared thermal imaging of P32L8 damaged spline for self-repair under NIR light irradiation (1.61 W cm^{-2}, 808 nm)
Movie S6.
The photo-thermal-mechanical conversion of P32L8 under xenon lamp irradiation (0.1W cm^{-2})
Movie S7.
The photo-thermal-mechanical conversion of POE under xenon lamp irradiation (0.1W cm^{-2})
Movie S8.
The photo-thermal-mechanical conversion of P32L8 under NIR light irradiation (1.072 W)
Movie S9.
The photo-thermal-mechanical conversion of P32L8 under NIR light irradiation (1.476 W)
Movie S10.
The photo-thermal-electric conversion of P32L8 under xenon lamp irradiation (1.476 W)
Movie S11.
The photothermal control switch based on photothermal conversion effect of lignin under NIR light irradiation (1.25 W cm^{-2}, 808 nm)

Table S1. Comparison of the photothermal efficiency (η_{PT}) of various materials.

Contrast Sample	Laser type (nm)	Power density (W cm^{-2})	η_{PT} (%)	Classification	Ref.
HAuNs	808	4	38.8	noble metal nanomaterials	10
Pd@Au bimetallic nanoplates	1064	0.96	56.9		11
AuNs	808	1.2	40.5		12
carbon produced from grape residue	Solar light	0.15	59.4	carbon nanomaterials	13
activated carbon nanoparticles	808	1.00	45.2		14
porous nanocarbon	808	1.00	40.0		15
Au-Cu_9S_5 NPs	1064	0.7	37	transition metal chalcogenide nanomaterials	16
Cu_9S_5 nanocrystals	980	0.51	25.7		17
PEGylated copper sulfide nanoparticles of CuS	806	0.18	71.4		18
BDPIN Boron dipyrromethene derivative	660	0.5	28.6	conjugated organic materials	19
TBDOPV-DT	1064	3.58	50.5		20
DPP-TPA	660	1	34.5		21
AOH	808	1.25	**53.7**	pristine lignin	This work
AL	808	1.25	**48.8**	pristine lignin	This work
P32L8	808	1.25	**40.2**	Lignin-based biocomposite	This work

REFERENCES AND NOTES

1. B. Delley, *J. Chem. Phys.*, 2000, **113**, 7756-7764.
2. J. P. Perdew, *Rev. Lett.*, 1996, **77**, 3865-3868.
3. B. Delley, *J. Chem. Phys.*, 1990, **92**, 508-517.
4. M. Dolg, U. Wedig, H. Stoll and H. Preuss, *J. Chem. Phys.*, 1987, **86**, 866-872.
5. A. Bergner, M. Dolg, W. Kuchle, *Mol. Phys.*, 1993, **80**, 1413-1441.
6. A. Bergner, M. Dolg, W. Kuchle, *J. Chem. Phys.*, 2010, **132**, 154104.
7. Y. Cao, J. Dou, N. Zhao, S. Zhang, Y. Zheng, J. Zhang, , J. Wang, J. Pei and Y. Wang, *Chem. Mater.*, 2017, **29**, 718-725.
8. D. K. Roper, W. Ahn and M. Hoepfner, *J. Phys. Chem. C.*, 2007, **111**, 3636-3641.
9. Y. Cao, Z. Wang, S. Liao, J. Wang and Y. Wang, *Chem. Eur. J.*, 2016, **22**, 1152-1158.
10. W. Choi, J. Y. Park, and Y. Kim, *J. Ind. Eng. Chem.,* 2021, **95**, 120-125.
11. Y. Zhang, F. Lv, Y. Cheng, Z. Yuan, F. Yang, C. Liu, Y. Cao, K. Zhang, H. Lu, S. Zada, S.

Guo, H. Dong, and X. Zhang, *Adv. Healthcare Mater*., 2020, **9**, 1901528.

12. L. Zhang, C. Liu, Y. Gao, Z. Li, J. Xing, W. Ren, L. Zhang, A. Li, G. Lu, A. Wu, and L. Zeng, . *Adv. Healthcare Mater*., 2018, **7**, 180114.
13. Q. Wang, L. Qiu, Y. Jia, Y. Chang, X. Tan, L. Yang, and H. Chen, *Sol. Energy Mater. Sol. Cells.,* 2019, **202**, 110-116.
14. G. Wu, B. Jiang, L. Zhou, A. Wang, and S. Wei, *J. Mater. Chem. B.,* 2021, **9**, 2447-2456.
15. Q. Wang, D. Niu, J. Shi, and L. Wang, *ACS Appl. Mater. Interfaces.,* 2021, **13**, 11683-11695.
16. X. Ding, C. Liow, M. Zhang, R. Huang, C. Li, H. Shen, M. Liu, Y. Zou, N. Gao, Z. Zhang, Y. Li, Q. Wang, S. Li, and J. Jiang, *J. Am. Chem. Soc.,* 2014, **136**, 44, 15684-15693.
17. Q. Tian, F. Jiang, R. Zou, Q. Liu, Z. Chen, M. Zhu, S. Yang, J. Wang, J. Wang, and J. Hu, *ACS.Nano*., 2011, **12**, 9761-9771.
18. R. Marin, A. Skripka, L. V. Besteiro, A. Benayas, Z. Wang, A. O. Govorov, P. Canton, and F. Vetrone, *Small*, 2018, **14**, 1803282.
19. D. Zou, A. Zhang, J. Chen, Z. Chen, J. Deng, G. Li, S. Zhang, Z. Feng, J. Feng, and J. Yang, *Mater. Chem. Front.* 2021, **5**, 2694-2701.
20. Y. Cao, J. Dou, N. Zhao, S. Zhang, Y. Zheng, J. Zhang, J. Wang, J. Pei, and Y. Wang, *Chem. Mate*r., 2017, **9**, 718-725.
21. Y. Cai, P. Liang, Q. Tang, X. Yang, W. Si, W. Huang, Q. Zhang, and X. Dong, *ACS Nano.,* 2017, **11**, 1054-1063.